



Synthesis of Graphene Nanoplatelet-Alginate Composite Beads and Removal of Methylene Blue from Aqueous Solutions

Ferda CİVAN ÇAVUŞOĞLU^{1,*} 

¹Istanbul Beykent University, Faculty of Engineering and Architecture, Department of Chemical Engineering, Istanbul, 34396, Turkey

Abstract: The discharge of various types of wastewater into natural streams leads to significant problems by increasing the toxicity of the wastewater. For this reason, methods and materials are being developed by researchers in line with effective, economic, and environmental principles. In this study, the removal of methylene blue, a toxic dyestuff, from aqueous solutions was investigated by synthesizing sodium alginate (SA) and graphene nanoplatelet-sodium alginate composite (SA-GNP) beads. The structural characteristics of the materials were analyzed using FTIR, TGA, optical microscope, and SEM methods. All parameters determining the efficiency of the methylene blue adsorption system were optimized in a batch system. The effects of various factors, such as adsorbent amount, contact time, adsorption temperature, dye concentration, solution pH, pHzpc values of SA and SA-GNP beads, presence of different ions, and beads swelling, on the adsorption process, were investigated. To investigate the mechanism of the adsorption system, the adsorption data were fitted to a non-linear form of the Langmuir, Freundlich, and Temkin equilibrium isotherm models, as well as the Pseudo-first-order (PFO), Pseudo-second-order (PSO), and Bangham kinetic models. High regression coefficients were achieved in the studied kinetic and isotherm models ($0.86 \leq R^2 \leq 0.99$), and the experimental data were found to be compatible with the model parameters. Maximum adsorption capacities (q_m) of 167.52 mg/g and 290.36 mg/g were obtained for the SA and SA-GNP adsorbents, respectively, at 308 K. The optimum temperature for both adsorption systems was found to be 308 K. The efficiency of methylene blue dyestuff removal was improved with graphene nanoplatelet-based adsorbents.

Keywords: Adsorption, alginate, graphene nanoplatelet, isotherm, kinetics, methylene blue.

Submitted: October 29, 2022. **Accepted:** February 20, 2023.

Cite this: Civan Çavuşoğlu F. Synthesis of Graphene Nanoplatelet-Alginate Composite Beads and Removal of Methylene Blue from Aqueous Solutions. JOTCSA. 2023;10(2):287-302.

DOI: <https://doi.org/10.18596/jotcsa.1196282>.

***Corresponding author. E-mails:** ferda.cvn@gmail.com; ferdacavusoglu@beykent.edu.tr.

1. INTRODUCTION

Ground and surface waters are polluted by wastewater from industrial, urban and agricultural sources. Due to rapid population growth and industrialization, the demand for clean water is increasing day by day (1). Synthetic dyes are pigments used in industries to color various products. It is widely used in many industries such as textile, plastic, paint, food, paper, cosmetics, medicine, and leather, and the wastewater of these sectors contains significant amounts of dyestuffs (2-4). The textile industry is the primary source of dyes, and today more than 10,000 dyes and

pigments are used for this purpose (5,6). The discharge of colored wastewater, which has a toxic effect and is resistant to degradation in the aquatic environment, into natural streams causes many serious problems by increasing the toxicity of the wastewater and the chemical oxygen demand (COD) (4,6).

Methylene blue (MB), which is in the cationic dye class, has many industrial applications (6-8). It is considered an important harmful organic pollutant in the aquatic environment due to its toxicity, carcinogenicity, mutagenicity, and non-biodegradability (7). Exposure can cause respiratory

complications, increased heart rate, nausea, profuse sweating, jaundice, and tissue necrosis (1,6,8). Various biological and physicochemical methods such as ultrafiltration, nanofiltration, coagulation, precipitation, membrane processes, ion exchange, electrolysis, biological processes, chemical oxidation, and adsorption are used in the removal of dyestuffs from wastewater (2,5,9).

The adsorption process is considered a versatile method for the removal of environmental pollutants from aqueous solutions with its low cost, simple and easy separation method, fast and environmentally friendly features (7,8). It also does not require sludge formation; adsorbents can be regenerated and reused (2). In recent years, various studies have been carried out to develop materials that can be used as low-cost and environmentally friendly adsorbents in wastewater treatment applications. Natural resource-based adsorbents such as activated carbon, zeolite, clay, and synthetic polymers are the materials used for this purpose. Among the biopolymers of interest, alginate and its cross-linked derivatives are well-known polysaccharide-based materials (9,10). It is an environmentally friendly natural carbohydrate polymer composed of sodium alginate (SA), mannuronic acid, and guluronic acid (7). Adsorbents derived from natural polymers are widely used in the removal of dyes from wastewater due to their abundance, low cost, non-toxicity, biocompatibility, biodegradability, abundant carboxyl and hydroxyl groups, hydrophilicity and recyclability (1,7,9). Due to its negative charge, alginate is seen as a suitable polymer that can be used in the removal of heavy metals and cationic dyestuffs. Studies have shown that using alginate in the form of nanocomposites with materials such as graphene, Fe_3O_4 , and montmorillonite contributes to the improvement of both the mechanical properties of alginate and its adsorption properties (4). Compositing graphene with polymeric materials increases the possibility of adding new functional groups to the surface, as well as increasing the number of active sites to fix a large number of organic and inorganic contaminants (11).

Recently, many studies have used graphene-based materials for the adsorption of different pollutant components from water (12,13). Graphene, which is a two-dimensional allotrope of carbon, is used in many fields due to its large specific surface area and biocompatibility, electronic, chemical, and thermal properties, removal of drugs and organic pollutants, and its suitability for use in composite material production. Having a good strength structure and being environmentally compatible, graphene-derived composite materials (graphene oxide, graphene nanoplatelets-GNPs, etc.) are preferred in environmental technologies of the removal of pollutants from water (13–15).

In recent studies, many graphene-polymer composites have been synthesized and used in the removal of various pollutants by the adsorption method (7,10,11,16–21). In this study, SA and SA-GNP beads were synthesized and used as an adsorbent for the removal of methylene blue from aqueous solutions by the adsorption method. In order to improve the adsorption properties, an SA-GNP composite was prepared by adding GNP to the bead formulation. The characterizations of the synthesized adsorbents were conducted by FTIR, TGA, optical microscope and SEM methods. The effects of different parameters such as adsorbent amount, dyestuff concentration, solution pH, pHzpc values, presence of different ions (NaCl), contact time, and adsorption temperature on the adsorption system were investigated, and optimum conditions were determined. In addition, the effect of swelling of the beads on the adsorption capacity was investigated by looking at the swelling behavior of the adsorbent beads. Langmuir, Freundlich, and Temkin isotherm equilibrium models and PFO, PSO, and Bangham kinetic models were fitted with experimental data, and the mechanism of the adsorption system was examined and interpreted.

2. MATERIALS AND METHODS

2.1. Materials

GNP (thickness 1–20 nm, width: 1–50 μm) from XG Science (xGnP®-C-750), sodium alginate from Sigma-Aldrich, CaCl_2 , methylene blue (MB) ($\text{C}_{16}\text{H}_{18}\text{ClN}_3\text{SxH}_2\text{O}$ ($x=2-3$)), HCl (36.5%), NaOH (≥ 99) and NaCl were obtained from Merck. High-purity water obtained from the Millipore Direct-Q3 water treatment system was used in all experimental stages.

2.2. Synthesis of Materials

To synthesize materials, 2% (w/v) sodium alginate solution was mixed thoroughly in a magnetic stirrer and prepared separately for SA and SA-GNP composite beads. In synthesizing GNP-based composite material (SA-GNP), 50 mg GNP was added to the prepared 2% sodium alginate solution and mixed again in the magnetic stirrer until a homogeneous mixture was obtained. This suspension mixture was slowly added to the 2% CaCl_2 solution prepared in a volume of 100 mL with the help of a dropper to form beads in a spherical shape. After being kept in solution for gelatinization for 24 hours, the obtained materials were filtered off and washed several times with distilled water to separate them from CaCl_2 . Then, the prepared beads were kept in a vacuum oven at 30°C for 3 hours to allow them to dry. It has been seen in the literature that partial drying of the prepared materials reduces the porosity of the beads, while complete dehydration can cause surface cracking, which can facilitate the surface erosion of the material upon rehydration. Temperature is important as it can affect the swelling behavior of

the beads (22). Synthesis of SA adsorbent without GNP additive was carried out similarly. Prepared SA and SA-GNP materials were stored in a desiccator

for use in studies. The preparation of SA and SA-GNP beads is schematically presented in Figure 1.



Figure 1: Preparation of SA and SA-GNP beads.

2.3. Characterization of Materials

Surface characterizations of SA and SA-GNP adsorbents were performed using Fourier transform infrared spectroscopy (FTIR), thermogravimetric analysis (TGA), optical microscope, and Scanning electron microscopy (SEM) methods. FTIR analysis (Bruker Alpha) was performed to determine the structural properties; the KBr method was used by recording the IR spectra between 400-4000 cm^{-1} . TGA (Hitachi STA-7200) measurements were carried out by taking samples in the range of 5-10 mg and heating them at a rate of 10°C/min under a nitrogen atmosphere (200 mL/min) in the temperature range of 25°C-1000°C. The morphology of the beads was observed with a scanning electron microscope (TESCAN VEGA 3) at 10 kV and 100x magnification. Before analysis, the surface of the samples was sputter coated with a gold-palladium layer for SEM visualization.

Additionally, The morphology of the beads was visually examined using an OLYMPUS microscope (CKX53, Japan), and digital images were obtained. Information about the color, shape, and texture of the surface of the beads was obtained, and the diameter of the beads was measured. Besides, a swelling test was applied to the prepared adsorbent beads, and its effect on the adsorption process was investigated.

2.4. Adsorption Studies

Adsorption studies were carried out batch-wise in an incubator shaker. To determine the optimum adsorption conditions, the effects of different process variables such as adsorbent amount, contact time, dyestuff concentration, temperature, pH and foreign ion effect (NaCl) on adsorption were investigated. Different parameter ranges (adsorbent amount 0.1-1 g/L, contact time 0-180 min, dyestuff concentration 1-25 mg/L, temperature 298-318 K, pH value 3-11, NaCl molar concentration 0.005-0.1 M) based experiments were carried out. The MB dyestuff solution volume was kept constant at 10 mL in all experiments. In experimental studies, all concentrations of adsorbate solutions were

measured at 665 nm with a UV-Vis spectrophotometer (Jasco V-730, Japan). Adsorption capacities (q_e , mg/g) and removal efficiencies (%) are respectively calculated using Equation 1 and Equation 2. In equations, C_0 (mg/L) dyestuff initial concentration, C_e (mg/L) equilibrium concentration, m (g) adsorbent amount, and V (L) solution volume.

$$q_e = \frac{(C_0 - C_e) \cdot V}{m} \quad (\text{Eq. 1})$$

$$\% \text{ Percentage of removal} = \frac{(C_0 - C_e)}{C_0} \times 100 \quad (\text{Eq. 2})$$

The point of zero charge (pH_{PZC}) values of the adsorbent materials were determined by the pH drift method. The pH of 0.01 M NaCl solution was adjusted to different pH values (4, 6, 8, 10, and 12) with 0.1 M NaOH and 0.1 M HCl solutions. Mixtures of approximately 1.5 mg of SA and SA-GNP beads and 20 mL of NaCl solution were kept in a shaking incubator at 25°C for 24 hours. After this process, the final pH values of samples were measured by pH meter, and a graph was drawn between the initial and final pH values, and the diagonal intersection point was accepted as pH_{PZC} (23,24).

3. RESULTS AND DISCUSSIONS

3.1. Characterization Results

FTIR, TGA, and SEM methods were applied to characterize the prepared alginate-based adsorbent beads, and their morphology was examined by obtaining digital images with an optical microscope. The FTIR spectra of SA and SA-GNP adsorbents measured in the 400-4000 cm^{-1} range before and after adsorption are shown in Figure 2. FTIR spectra of alginate-based adsorbents show similar peaks before and after adsorption for both adsorbents. Specified wavelengths indicate the presence of

groups at 1028 and 1037 cm^{-1} (C-O-C stretching frequency), 1410, 1430 cm^{-1} , and 1637 cm^{-1} (symmetric and asymmetric stretching COO^-), 2922 and 2926 cm^{-1} (C-H stretching vibration), 3445 and 3450 cm^{-1} (-OH stretching vibration) (25–28). It

was observed that the intensity of these peaks after adsorption decreased compared to before adsorption. It is thought that the MB dyestuff attaches to the functional groups herein.

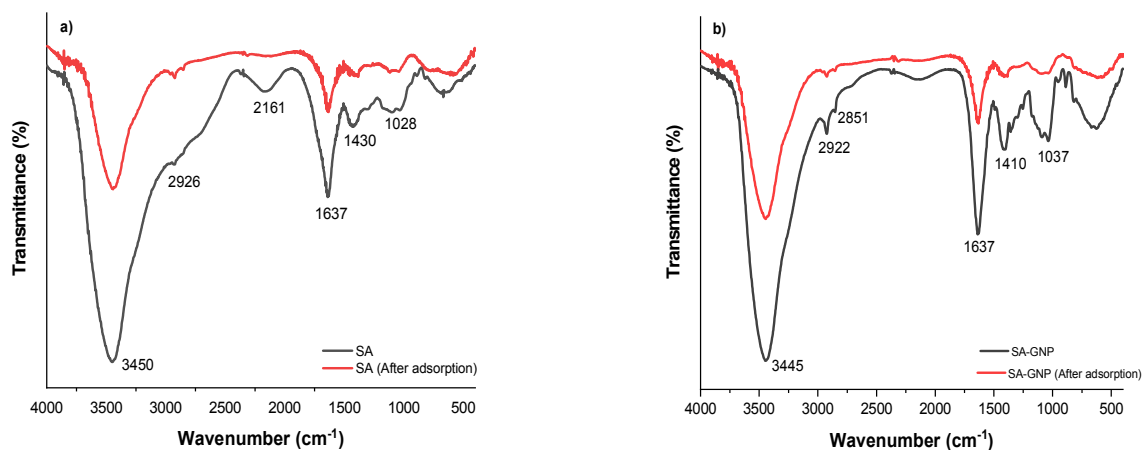


Figure 2: FTIR plots of SA (a) and SA-GNP (b) before and after adsorption.

TGA plots of SA and SA-GNP are shown in Figure 3. The thermal behavior of adsorbents is similar, and their thermal decomposition takes place in the temperature region of 200°C to 500°C. The weight loss in the first stage is attributed to the removal of

volatile products such as physically adsorbed water (29,30). The decomposition temperature at 10% weight loss was calculated as 189°C and 197°C for SA and SA-GNP adsorbents, respectively.

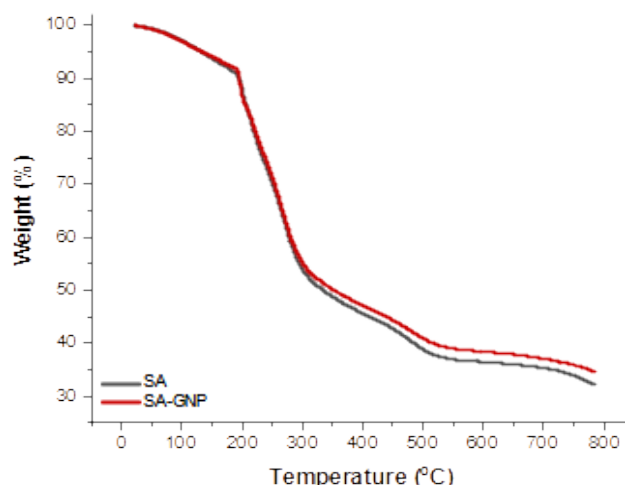


Figure 3: TGA curves of SA and SA-GNP.

Weight loss in the second stage is attributed to the decrosslinking of the polymer networks (29). The region responsible for the large weight loss shows the degradation of the carboxylic groups in the sodium alginate structure (in the temperature range of 178-190 °C). The thermal stability of the

materials is determined by the large loss of mass at which thermal decomposition begins, large changes are observed after exceeding 200 °C (31). From the data obtained at 800 °C, it is seen that the remaining material contents for SA and SA-GNP are 31% and 35% by weight (total weight),

respectively. According to the final thermal oxidative decomposition temperatures, it can be said that SA-GNP composite material has slightly higher thermal stability than SA. In this direction, it can be said that the GNP additive slightly increases the thermal stability of the material.

The morphological characterization of beads was observed using SEM. The obtained topographic

images of SA and SA-GNP are shown in Figure 4. The surfaces and sections of SA and SA-GNP showed a smooth and homogeneous morphology. GNP did not appear to cause any roughness or heterogeneity in the beads. It shows that the GNP is successfully dispersed by sonication and does not form agglomeration.

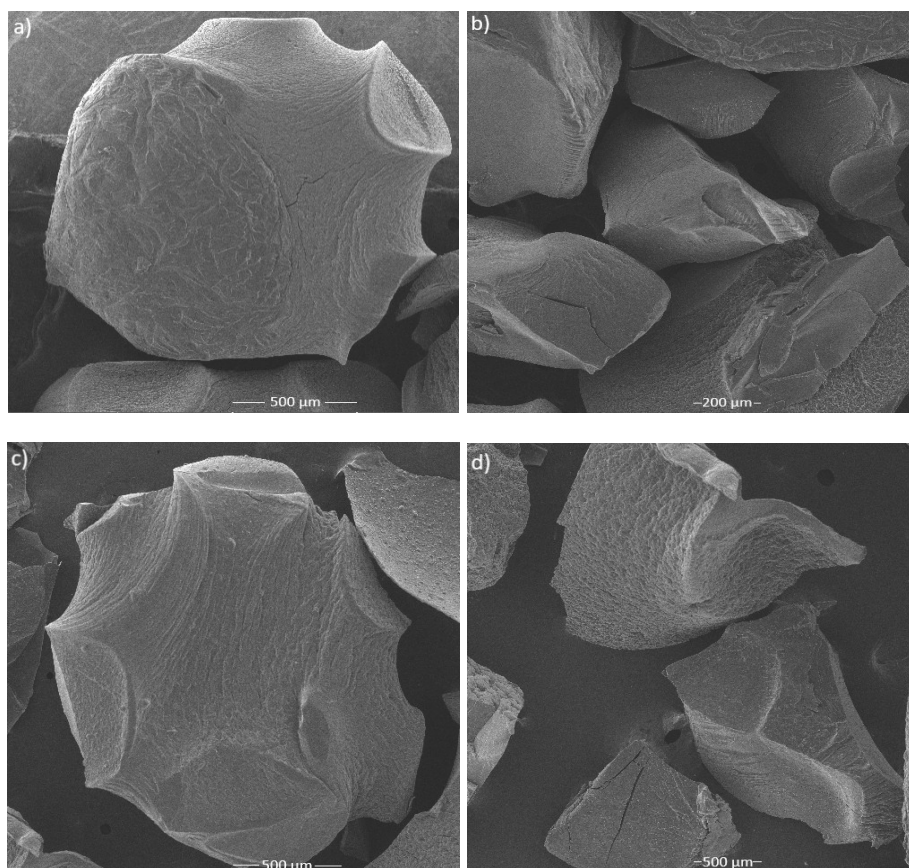


Figure 4: SEM images of SA (a,b) and SA-GNP (c,d) beads.

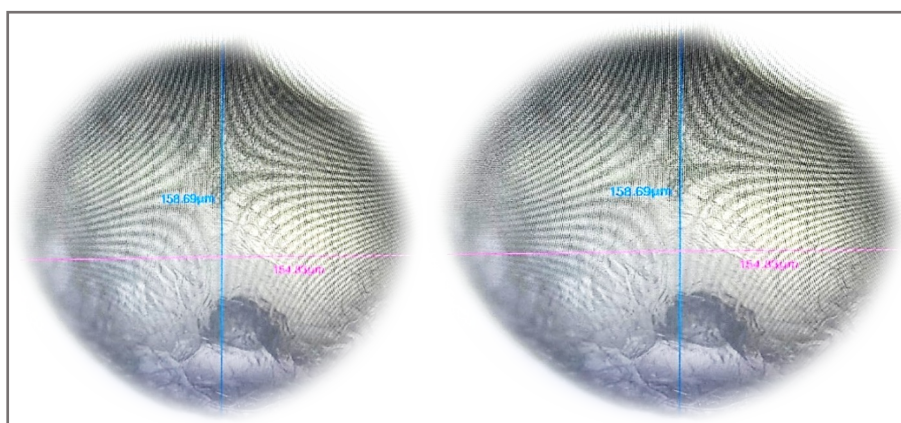


Figure 5: Digital images of SA and SA-GNP beads.

Additionally, the morphology of the beads was visually examined using an optical microscope, and

their digital images were obtained as in Figure 5. Information about the color, shape, and texture of

the surface of the beads was obtained, and the diameter of the beads was measured. The beads have a spherical shape and measure approximately 150 µm in diameter on average. SA beads are light yellow in color, while SA-GNP beads are black due to the color of the GNP.

The swelling behavior of adsorbent beads was determined gravimetrically in MB solution (pH=5.5) at 25°C. The percent swelling was calculated using Equation 3:

$$\% \text{Swelling} = \frac{(W_s - W_d)}{W_d} \times 100 \quad (\text{Eq. 3})$$

W_s is the weight of the swollen beads, and W_d is the weight of the dried beads. Swelling measurement continued until the swollen beads were adequately weighed. Although the beads had swelling properties, there was no change in the

percentage of dye removal of the swollen beads compared to the dry ones (32,33).

3.2. Adsorption Studies

3.2.1. Adsorption process variables

To investigate the effect of the amount of adsorbent, mixtures of adsorbents in 0.1, 0.25, 0.5, 0.75, and 1 g/L amounts and stock MB solution with an initial dye concentration of 10 mg/L were left to shake for 120 minutes, based on previous preliminary experiments. The calculated adsorption capacities of the experiments with different amounts of SA and SA-GNP adsorbents are shown in Figure 6. According to the experimental results, the highest removal efficiencies (%) of SA and SA-GNP were obtained as 71.55% and 74.59%, respectively. As the amount of adsorbent increased, the removal efficiency of the dyestuff increased. This is due to the grown surface area resulting from the rise in adsorbent mass and the increased number of active sites (34,35).

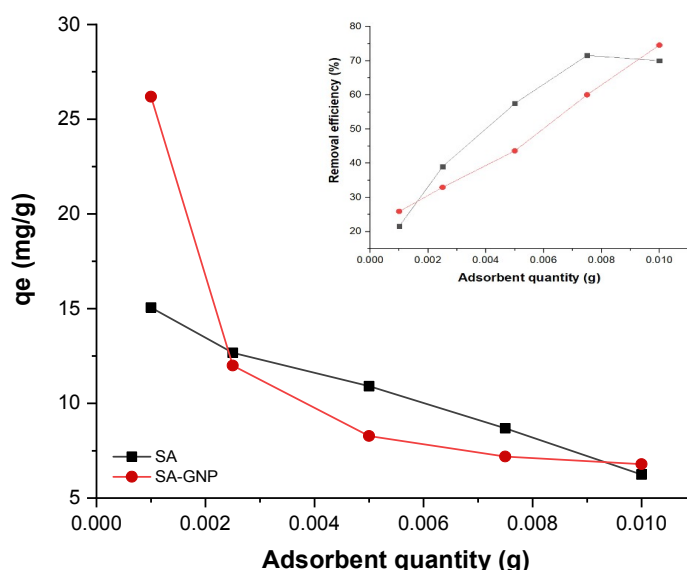


Figure 6: Effect of adsorbent dose on adsorption capacity and removal efficiency (inset).

As seen in Figure 6, the adsorption capacity decreased as the amount of adsorbent increased. The adsorption capacity values vary between 6.25–15.06 mg/g for SA, and 6.79–26.19 mg/g for SA-GNP. As the adsorbent dose decreased, the amount of MB solution per gram of adsorbent increased. This may be because all active sites in the adsorbent are fully exposed to MB and utilized at a lower adsorbent dose, and only some of the active sites are exposed and occupied by MB at a higher adsorbent dose (35). The highest adsorption capacity was obtained at 0.1 g/L adsorbent concentration as 15.06 mg/g for SA and 26.19 mg/g

for SA-GNP. Based on these data, the optimum amount of adsorbent was chosen as 0.1 g/L.

To determine the equilibrium time of the adsorbents, experiments were carried out with MB solution for 1, 5, 10, 15, 30, 45, 60, 90, 120, and 180 minutes. Equilibrium times were determined, and the obtained data were also used for kinetic modeling calculations. The calculated adsorption capacities of the experiments performed with SA and SA-GNP adsorbents at different times are shown in Figure 7.

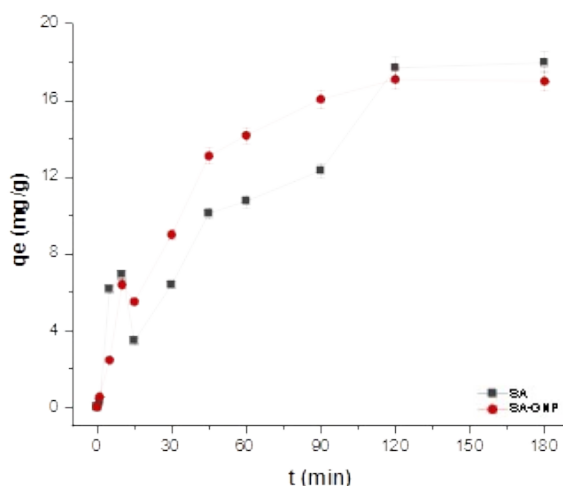


Figure 7: Effect of contact time on adsorption capacity.

Equilibrium times of the adsorption systems were determined at room temperature. The fast adsorption in the first stage can be explained by the high driving force that provides rapid mass transfer of MB ions to the adsorbent surface, as well as the high number and availability of active sites in the adsorbent (36). Both adsorption systems reached equilibrium after approximately 120 minutes, and it was observed that there were no major changes in adsorption capacity after this point. Based on these data, 120 minutes was chosen as the optimum contact time, and the q_e values for SA and SA-GNP adsorbents were obtained as 17.97 mg/g and 17.00 mg/g, respectively.

The effect of MB solution at different pH values on adsorption was investigated by adjusting the pH values to 3, 5, 7, 9, and 11 with 0.1 M HCl and 0.1 M NaOH solutions. Calculated adsorption capacities of the experiments with SA and SA-GNP adsorbents at different pH values are shown in Figure 8 (a). The q_e values ranged from 48.16 – 67.52 mg/g for SA and 50.95–97.29 mg/g for SA-GNP; that is, the amount of MB solution per gram adsorbent decreased as pH increased. These results show that an acidic solution is more suitable for the MB adsorption system. Since the surface of sodium alginate is negatively charged up to pH 7, the

presence of H^+ ions at low pH values increased the adsorption capacity value (37). According to the literature, this shows that the cationic dyestuff can be better ionized at low pH values and is based on the interaction of more dye molecules with the adsorbent (38). The highest adsorption capacities were obtained at pH 3, 67.52 mg/g for SA and 97.29 mg/g for SA-GNP.

The surface charge properties of adsorbents at different pH values significantly affect their adsorption capacity. Additionally, the pH_{pzc} was determined to evaluate the surface electrification of adsorbents in the solution. As seen in Figure 8 (b), experimental pH_{pzc} values of SA and SA-GNP were obtained as 5.26 and 5.11, respectively. In the pH range of 3-10, an increase in the negative charge of the adsorbent surface due to deprotonation of the carboxyl group increased the electrostatic attraction between the cationic MB, thereby increasing the adsorption capacity of SA and SA-GNP beads (24). In the study, SA and SA-GNP beads showed efficient adsorption on MB from an aqueous solution in the initial pH range of 4-7. The normal pH of the MB solution is also about 6.06 ($T=27.5^\circ C$), so no pH adjustment was required for the other experiments, and the MB initial pH value is in optimum conditions for the study.

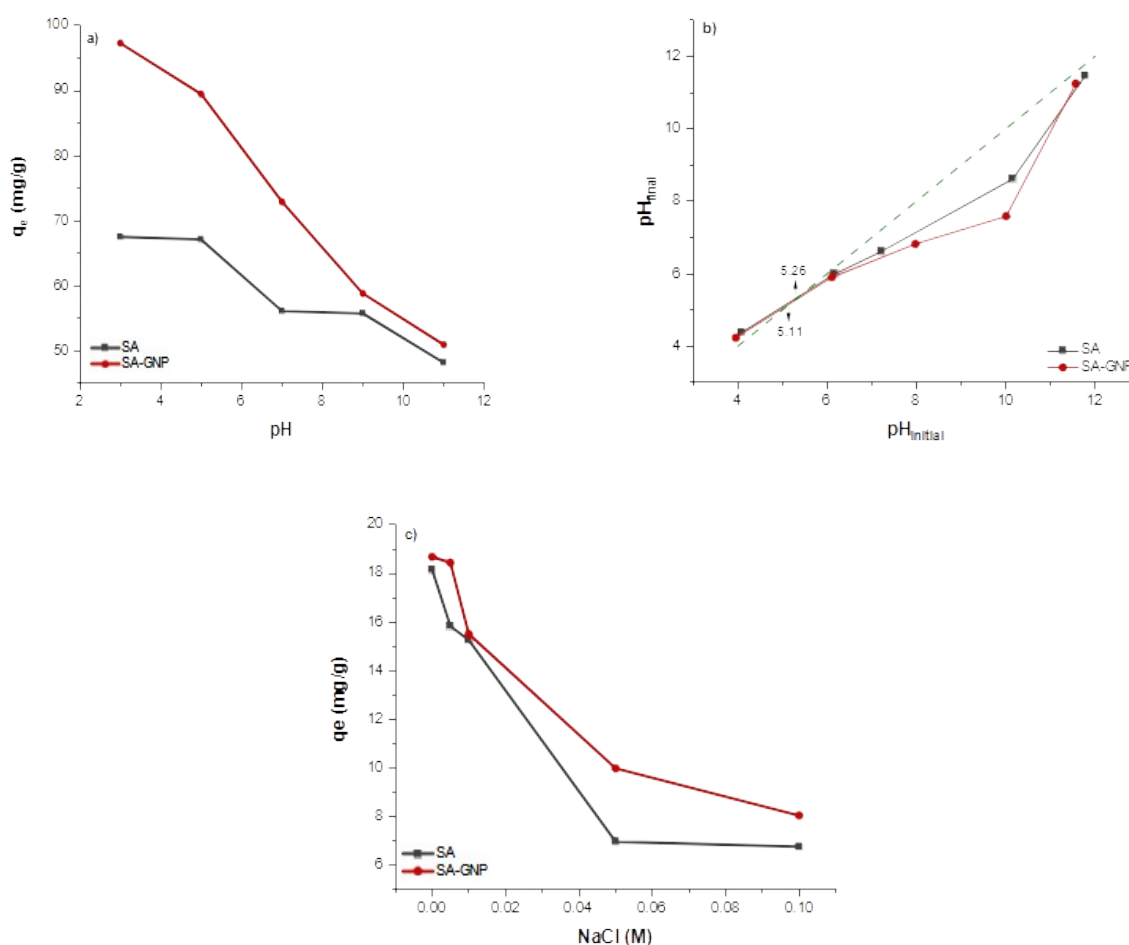


Figure 8: Effect of pH (a) on adsorption capacity, pH_{ZPC} plots of SA and SA-GNP (b), and foreign ion-NaCl (c) on adsorption capacity.

It is known that different polluting ions present with MB dyestuff in adsorption processes also affect adsorption. In this study, NaCl was chosen as a different foreign ion, and its effect on adsorption capacity with MB was investigated. While MB concentration was 10 mg/L, NaCl concentrations were prepared as 0.005, 0.01, 0.05, and 0.1 M. The graph of Figure 8 (c) shows the adsorption capacity values obtained at different NaCl concentrations of SA and SA-GNP adsorbents. As the molar concentration of NaCl increased, the adsorption capacity values decreased. The adsorption capacity of SA decreased from 15.83 mg/g (0.005 M) to 6.76 mg/g (0.1 M). The adsorption capacity of SA-GNP decreased from 18.43 mg/g (0.005 M) to 8.05 mg/g (0.1 M). This result is thought to be related to the competition of cation ions and Na^+ of MB for adsorption sites (34).

3.2.2. Adsorption kinetic models

Adsorption kinetics were investigated by using experimental data obtained at different times in the adsorption of SA and SA-GNP adsorbents and MB

dyestuff. The adsorption data were fitted to a non-linear form of PFO (Equation 4), PSO (Equation 5), and Bangham (Equation 6) (23) kinetic models. The graphs of all adsorption systems are shown in Figure 9, and the calculated model parameters are presented in Table 1.

In equations, q_t (mg/g) adsorption capacity at time t , k_1 (min^{-1}) PFO kinetic model rate constant, k_2 (g/mg.min) PSO kinetic model rate constant, k Bangham constant, u Bangham parameter and t (min) is the contact time.

$$q_t = q_e \cdot (1 - e^{-k_1 \cdot t}) \quad (\text{Eq. 4})$$

$$q_t = \frac{q_e^2 \cdot k_2 \cdot t}{1 + k_2 \cdot q_e \cdot t} \quad (\text{Eq. 5})$$

$$q_t = k \cdot t^u \quad (\text{Eq. 6})$$

According to the parameters and R^2 values of the models, the kinetic models for both adsorption

systems fit well with the experimental data (SA; $R^2 \geq 0.87$, SA-GNP; $R^2 \geq 0.92$), which are consistent with previous studies (36,39). The R^2 values of the PFO and PSO kinetic models show that both adsorption systems fit the PSO kinetic model better. The reaction mechanisms between adsorbent and adsorbate depend on chemical adsorption, including the sharing or exchanging of electrons as covalent forces and valence forces via ion exchange (40). The kinetic model rate (k_1 , k_2) obtained from the models showed that the adsorption process performed with SA-GNP/MB was faster than the

SA/MB adsorption system (SA: $k_1=0.0168 \text{ min}^{-1}$, $k_2=0.0007 \text{ g/mg.min}$; SA-GNP: $k_1=0.0417 \text{ min}^{-1}$, $k_2=0.0028 \text{ g/mg.min}$). Experimental data and model parameters of adsorption capacity were found to be compatible with each other.

Bangham model is a generalization of the Weber-Morris model and can be used to explain pore diffusion mechanisms. R^2 values (≥ 0.92) are high for both adsorption systems. The Bangham model shows that rate-controlled step adsorption of MB on SA and SA-GNP is pore diffusion (23).

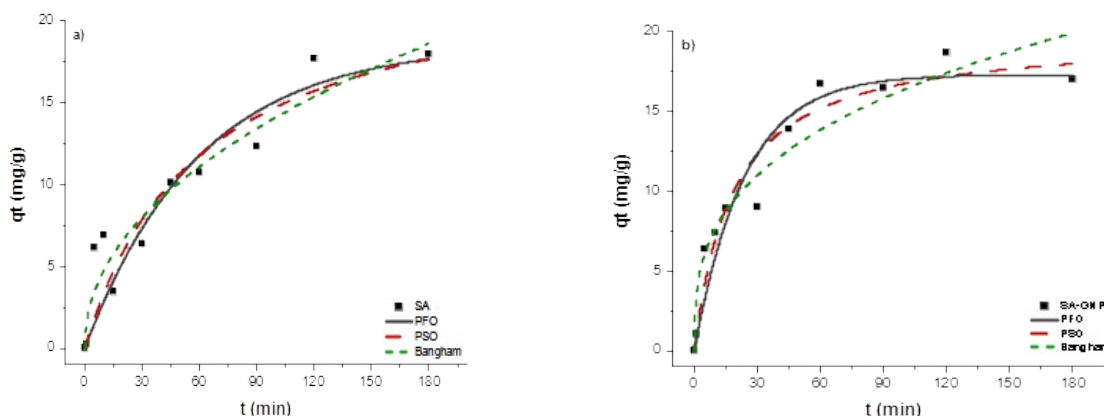


Figure 9: PFO, PSO, and Bangham kinetic models of SA (a) and SA-GNP (b).

Table 1: Kinetic model parameters of SA and SA-GNP.

MB Adsorption		SA	SA-GNP
PFO	q_e (mg/g)	18.58	17.302
	k_1 (min^{-1})	0.0168	0.0417
	R^2	0.87	0.93
PSO	q_e (mg/g)	23.60	19.815
	k_2 (g/mg.min)	0.0007	0.0028
	R^2	0.88	0.95
Bangham	k	1.617	3.569
	u	0.4705	0.3311
	R^2	0.92	0.93

MB concentration: mg/L

3.2.3. Adsorption equilibrium models

The effects of MB concentration and temperature on the adsorption process were investigated. Adsorption mechanisms and equilibrium conditions were examined using experimental data obtained at different temperatures for the adsorption of SA and SA-GNP adsorbents and MB dyestuff. Optimum adsorption temperatures were determined, and maximum adsorption capacities were calculated using the data obtained for isotherm model calculations. The adsorption data were fitted to a non-linear form of Langmuir (Equation 7),

Freundlich (Equation 8) (23), and Temkin (Equation 9) (41) equilibrium isotherm models. The graphs of all adsorption systems are shown in Figures 10 and 11, and the calculated model parameters are presented in Table 2.

In equations, q_m (mg/g) maximum adsorption capacity, K_L (L/mg) Langmuir isotherm constant, K_F (mg/g).(L/mg) $^{1/n}$ Freundlich isotherm constant, heterogeneity factor showing $1/n$ adsorption density, A_T Temkin isotherm equilibrium binding

constant, b_T isotherm constant, R (J/mol.K) gas constant, T (K) absolute temperature.

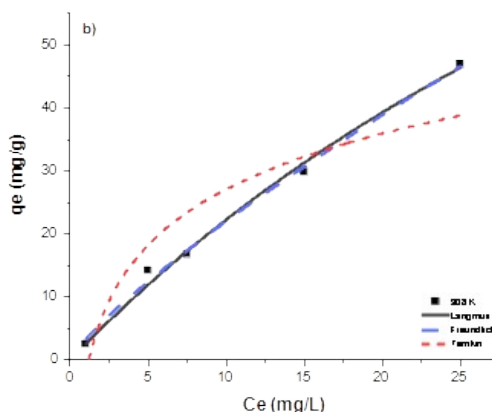
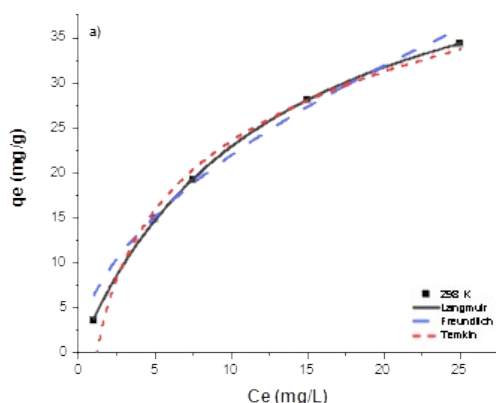
$$q_e = \frac{K_L q_m C_e}{1 + K_L C_e} \quad (\text{Eq. 7})$$

$$q_e = K_F C_e^{1/n} \quad (\text{Eq. 8})$$

$$q_e = \frac{R \times T}{b_T} \times \ln(A_T \times C_e) \quad (\text{Eq. 9})$$

According to the parameters and R^2 values of Langmuir and Freundlich models, the isotherm models for both adsorbent-MB adsorption systems fitted very well with the experimental data ($R^2 \geq 0.98$). Maximum adsorption capacities (q_m) for SA and SA-GNP were obtained in the range of 39.05-167.52 mg/g and 63.67-290.36 mg/g, respectively. While the q_m value for the SA-MB adsorption system was 167.52 mg/g at 308 K, the q_m for the SA-GNP-MB adsorption system was calculated as 290.36 mg/g at 308 K.

The maximum adsorption capacities obtained in similar studies in the literature are presented in Table 3. Compared to the literature, very efficient results were obtained in MB removal. Freundlich isotherm generally represents heterogeneous adsorption systems, and it is known that the adsorption process is suitable when the n parameter is between 1 and 10. MB removal is successful in applied adsorption processes since n values for both adsorption systems vary between 1.11-1.86. In other words, $1/n < 1$ indicates that the adsorption mechanism depends on chemisorption. It is known that the heterogeneity of the systems increases as the $1/n$ value approaches zero (40), and the highest heterogeneity in the investigated adsorption systems was obtained at 308 K for both adsorbents. The optimum temperature of the adsorption systems is 308 K, and the maximum adsorption capacities were obtained at this temperature value. The Temkin isotherm model indirectly describes the effects of adsorbent/adsorbate interactions. In this model, it is assumed that the heat of adsorption of all molecules decreases linearly with increasing coverage of the adsorbent (42). The Temkin model shows that the adsorption of MB dyestuff with SA and SA-GNP adsorbents is based on a chemisorption process.



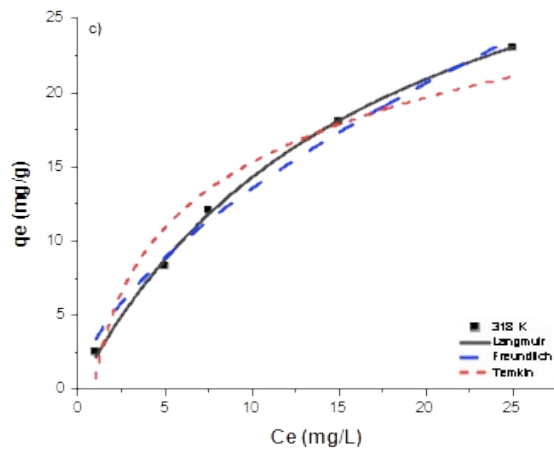


Figure 10: Langmuir, Freundlich, and Temkin isotherm models of SA, 298 K (a), 308 K (b), 318 K (c).

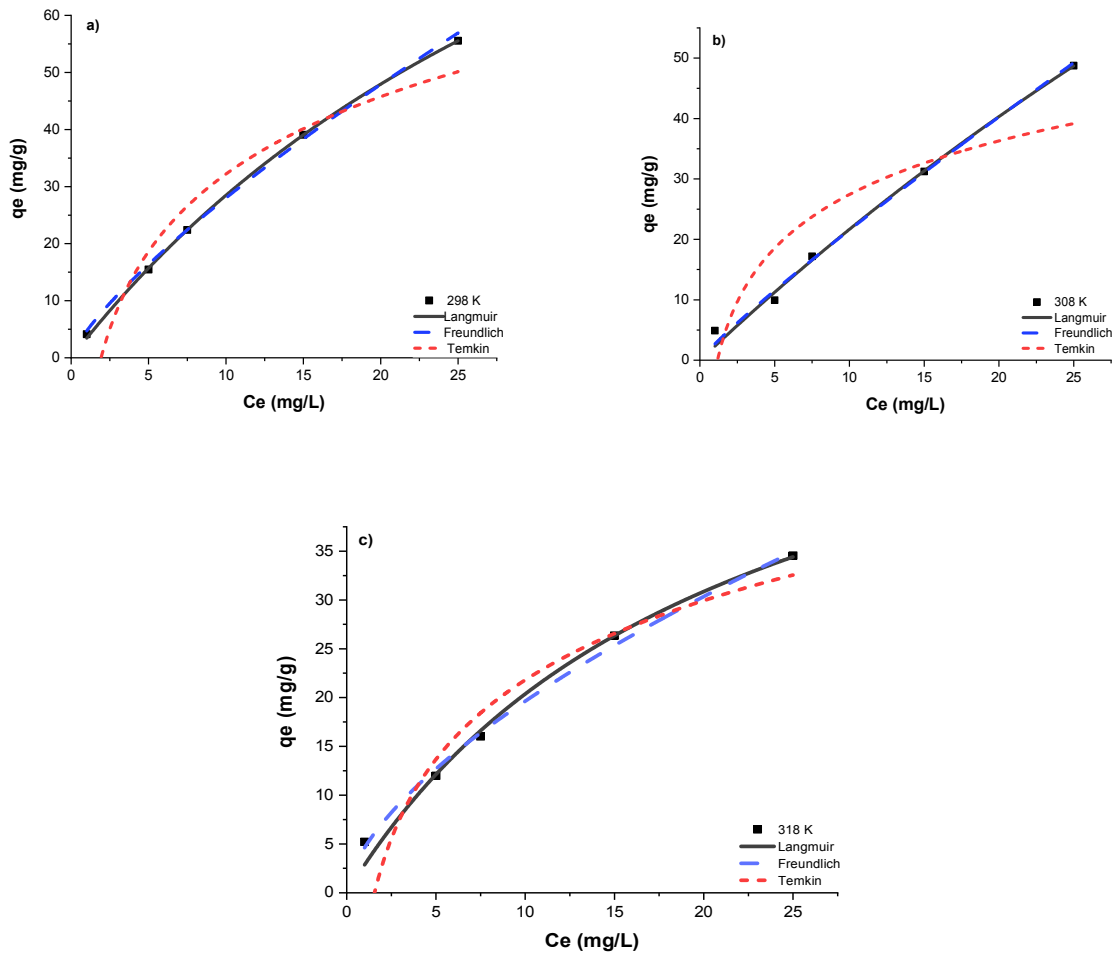


Figure 11: Langmuir, Freundlich, and Temkin isotherm models of SA-GNP, 298 K (a), 308 K (b), 318 K (c).

Table 2: Langmuir, Freundlich, and Temkin isotherm parameters.

MB Adsorption	SA			SA-GNP		
	298 K	308 K	318 K	298 K	308 K	318 K
Langmuir						
q_m (mg/g)	51.52	167.52	39.05	151.79	290.36	63.67
K_L	0.080	0.015	0.058	0.023	0.008	0.047
R^2	0.99	0.99	0.99	0.99	0.99	0.99
Freundlich						
K_F	6.36	3.34	3.33	4.71	2.70	4.62
n	1.86	1.22	1.64	1.29	1.11	1.59
R^2	0.98	0.99	0.99	0.99	0.99	0.99
Temkin						
A_T	0.837	0.833	1.12	0.518	0.851	0.641
b_T	223.7	200.4	418.2	126.6	199.9	225.2
R^2	0.98	0.86	0.94	0.94	0.79	0.97

Table 3: Summary of similar studies in the literature on methylene blue removal with composite alginate materials.

Adsorbents/Composite materials	Maximum adsorption capacities, q_m	References
Activated carbon-alginate beads	230 mg/g	(2)
Activated carbon, copper ferrite and alginate composites	400 mg/g	(9)
Activated carbon-alginate beads	769.23 mg/g	(43)
Bentonite-encapsulated alginate beads	2041 mg/g	(44)
Graphene oxide-magnetite nanocomposite	172.6 mg/g	(3)
Graphene oxide-montmorillonite/sodium alginate aerogel beads	150.66 mg/g	(7)
Graphene oxide/alginate quasi-cryogel beads	122.26 mg/g	(10)
Magnetic sodium alginate-modified zeolite adsorbent	181.85 mg/g	(24)
Magnetic alginate beads	38.9 mmol/g	(45)
Magnetic microspheres with sodium alginate and activated carbon	222.3 mg/g	(46)
Metal-organic framework (MOF)-based alginate composite beads	490.72 mg/g	(47)
Sodium alginate beads, SA	167.52 mg/g	This work
Graphene nanoplatelet composite beads, SA-GNP	290.36 mg/g	

4. CONCLUSIONS

SA and SA-GNP composite beads were synthesized as adsorbent material, and studies were carried out on the removal of MB from aqueous solutions by the adsorption method. Structural characterizations of the synthesized adsorbents are compatible with the literature. Optimum conditions for the adsorption system were determined by investigating the effects of different parameters such as adsorbent dose, MB dyestuff concentration, solution pH, presence of different ions (NaCl), beads swelling, contact time, and adsorption temperature. According to the results:

- An adsorbent dose of 0.1 g/L was determined as the optimum amount of adsorbent. At the end of the adsorption period of 120 minutes, the system reached equilibrium, and the optimum contact time for the experiments was determined as 120 minutes.
- In different pH experiments, high adsorption capacities were obtained at low pH (≤ 7) values, so the pH value of the MB solution (pH=6.06; T=27°C) is suitable for adsorption studies, and no pH adjustment has been made. In addition, in order to see the effect of pH, the pH_{ZPC} values of SA and SA-GNP beads were obtained as 5.26 and 5.11, respectively, by using the drift method. The effect of the presence of a different ion, NaCl, on the adsorption process was investigated, and the

adsorption capacity values decreased as the NaCl concentration increased.

- The mechanism of the adsorption system was investigated and interpreted. The adsorption data were fitted to a non-linear form of Langmuir, Freundlich, and Temkin equilibrium isotherm models and PFO, PSO, and Bangham kinetic models. High regression coefficients ($0.86 \leq R^2 \leq 0.99$) were obtained with the studied kinetic and isotherm models, and the experimental data were found to be compatible with the model parameters.
- The maximum adsorption capacities (q_m) of SA and SA-GNP adsorbents were obtained as 167.52 and 290.36 mg/g at 308 K, respectively, and the optimum temperature was 308 K for both adsorption systems.
- Despite the very low amount of GNP in SA-GNP adsorbent, it significantly increased the adsorption capacity and improved the adsorption process. Also, the addition of GNP slightly increased the thermal stability of SA-GNP.
- The spherical shape of the adsorbents did not require extra filtration and allowed them to be easily separated from the adsorbates. In this direction, simple operating convenience is provided to the adsorption process.

In conclusion, SA and SA-GNP were found to be economical, effective, and environmentally friendly adsorbents that can be used for the removal of MB from aqueous solutions.

5. CONFLICT OF INTEREST

The author declares no conflict of interest.

6. REFERENCES

1. Balçık Canbolat Ç, Özbey B. Production of cellulose nanocrystalline additive alginate adsorbent for the removal of organic dyes from aqueous solutions and investigation of dye removal efficiency. *Düzce University J of Science and Techn.* 2021;10:300–8. Available from: <DOI>.
2. Nasrullah A, Bhat AH, Naeem A, Isa MH, Danish M. High surface area mesoporous activated carbon-alginate beads for efficient removal of methylene blue. *Int J Biol Macromol.* 2018;107:1792–9. Available from: <DOI>.
3. Meral K, Metin Ö. Graphene oxide-magnetite nanocomposite as an efficient and magnetically separable adsorbent for methylene blue removal from aqueous solution. *Turkish J Chem.* 2014;38(5):775–82. Available from: <DOI>.
4. Okur M, Aktı F, Çetintaş A. Use of Polyaniline/Alginate Composite Material in the Adsorption of Acid Violet 90 Dye: Kinetics and Isotherm Evaluation. *Gazi University J of Science Part C: Design and Techn.* 2018;6(4):729–40. Available from: <DOI>.
5. Khan IA, Hassan MIU, Hussain H, Shah SM, Yasin T. Fabrication and characterization of amidoxime-functionalized silica decorated with copper: A catalytic assembly for rapid reduction of dyes. *Turkish J Chem.* 2021;45(2):410–9. Available from: <DOI>.
6. Hameed BH, Ahmad AA. Batch adsorption of methylene blue from aqueous solution by garlic peel, an agricultural waste biomass. *J Hazard Mater.* 2009;164(2–3):870–5. Available from: <DOI>.
7. E T, Ma D, Yang S, Hao X. Graphene oxide-montmorillonite/sodium alginate aerogel beads for selective adsorption of methylene blue in wastewater. *J Alloys Compd.* 2020;832:154833. Available from: <DOI>.
8. Borghei SA, Zare MH, Ahmadi M, Sadeghi MH, Marjani A, Shirazian S, et al. Synthesis of multi-application activated carbon from oak seeds by KOH activation for methylene blue adsorption and electrochemical supercapacitor electrode. *Arab J Chem.* 2021;14(2):102958. Available from: <DOI>.
9. Othman I, Abu Haija M, Kannan P, Banat F. Adsorptive removal of methylene blue from water using high-performance alginate-based beads. *Water Air Soil Pollut.* 2020;231(8). Available from: <DOI>.
10. Balkız G, Pingo E, Kahya N, Kaygusuz H, Bedia Erim F. Graphene oxide/alginate quasi-cryogels for removal of methylene blue. *Water Air Soil Pollut.* 2018;229(4). Available from: <DOI>.
11. Faysal Hossain MD, Akther N, Zhou Y. Recent advancements in graphene adsorbents for wastewater treatment: Current status and challenges. *Chinese Chem Lett.* 2020;31(10):2525–38. Available from: <DOI>.
12. Nigiz FU. Synthesis of a novel graphene-kaolin-alginate adsorbent for dye removal, and optimization of the adsorption by response surface methodology. *Res Chem Intermed.* 2019;45(7):3739–53. Available from: <DOI>.
13. Yusuf M, Elfgi FM, Zaidi SA, Abdullah EC, Khan MA. Applications of graphene and its derivatives as an adsorbent for heavy metal and dye removal: a systematic and comprehensive overview. *RSC Adv.* 2015;5(62):50392–420. Available from: <DOI>.
14. Madenli Ö, Devci EU, Gönen Ç. Graphene Applications in Heavy Metal Removal: Adsorption Technology. *Firat University J of Engineering Science.* 2021;33(1):151–9. Available from: <DOI>.

15. Zhang C, Chen Z, Guo W, Zhu C, Zou Y. Simple fabrication of Chitosan/Graphene nanoplates composite spheres for efficient adsorption of acid dyes from aqueous solution. *Int J Biol Macromol*. 2018;112:1048–54. Available from: <DOI>.
16. Bai C, Wang L, Zhu Z. Adsorption of Cr(III) and Pb(II) by graphene oxide/alginate hydrogel membrane: Characterization, adsorption kinetics, isotherm and thermodynamics studies. *Int J Biol Macromol*. 2020;147:898–910. Available from: <DOI>.
17. Wang Y, Pan J, Li Y, Zhang P, Li M, Zheng H, et al. Methylene blue adsorption by activated carbon, nickel alginate/activated carbon aerogel, and nickel alginate/graphene oxide aerogel: A comparison study. *J Mater Res Technol*. 2020;9(6):12443–60. Available from: <DOI>.
18. González-López ME, Laureano-Anzaldo CM, Pérez-Fonseca AA, Gómez C, Robledo-Ortiz JR. Congo red adsorption with cellulose-graphene nanoplatelets beads by differential column batch reactor. *J Environ Chem Eng*. 2021;9(2). Available from: <DOI>.
19. Ma J, Jiang Z, Cao J, Yu F. Enhanced adsorption for the removal of antibiotics by carbon nanotubes/graphene oxide/sodium alginate triple-network nanocomposite hydrogels in aqueous solutions. *Chemosphere*. 2020;242:125188. Available from: <DOI>.
20. Politaeva N, Yakovlev A, Yakovleva E, Chelysheva V, Tarantseva K, Efremova S, et al. Graphene oxide-chitosan composites for water treatment from copper cations. *Water*. 2022 Apr 29;14(9):1430. Available from: <DOI>.
21. Wang M, Li Y, Cui M, Li M, Xu W, Li L, et al. Barium alginate as a skeleton coating graphene oxide and bentonite-derived composites: Excellent adsorbent based on predictive design for the enhanced adsorption of methylene blue. *J Colloid Interface Sci*. 2022;611:629–43. Available from: <DOI>.
22. Bajpai SK, Sharma S. Investigation of swelling/degradation behaviour of alginate beads crosslinked with Ca²⁺ and Ba²⁺ ions. *React Funct Polym*. 2004;59(2):129–40. Available from: <DOI>.
23. Özçelik G, Civan Çavuşoğlu F, Özkara-Aydinoğlu Ş, Bayazit ŞS. Enhanced & effective phosphate recovery from water by indium fumarate & zirconium fumarate metal-organic frameworks: Synthesis, characterization, adsorption, kinetic and isotherm studies. *Surfaces and Interfaces*. 2022;29(December 2021). Available from: <DOI>.
24. Liu F, Li W, Zhou Y. Preparation and characterization of magnetic sodium alginate-modified zeolite for the efficient removal of methylene blue. *Colloids Surfaces A Physicochem Eng Asp*. 2021;629(May):127403. Available from: <DOI>.
25. Lacerda L, Parize AL, Fávère V, Laranjeira MCM, Stulzer HK. Development and evaluation of pH-sensitive sodium alginate/chitosan microparticles containing the antituberculosis drug rifampicin. *Mater Sci Eng C*. 2014;39(1):161–7. Available from: <DOI>.
26. Boddu A, Obireddy SR, Subbarao SMC, Rao KM, Venkata KRKS. Encapsulation of 5-Fluorouracil treated reduced graphene oxide in sodium alginate matrix for controlled and pH-responsive drug delivery. *ChemistrySelect*. 2021;6(25):6533–40. Available from: <DOI>.
27. Fan L, Du Y, Huang R, Wang Q, Wang X, Zhang L. Preparation and characterization of alginate/gelatin blend fibers. *J Appl Polym Sci*. 2005;96(5):1625–9. Available from: <DOI>.
28. Urzedo AL, Bernardes JS, Pedron T, Batista BL, Akiba N, Gaubeur I, et al. Synthesis and characterization of calcium alginate and cellulose nanocrystal films for lead removal. *J Phys Conf Ser*. 2019;1323(1). Available from: <DOI>.
29. Siddaramaiah, Swamy TMM, Ramaraj B, Lee JH. Sodium alginate and its blends with starch: Thermal and morphological properties. *J Appl Polym Sci*. 2008 Sep 15;109(6):4075–81. Available from: <DOI>.
30. Lu T, Xiang T, Huang XL, Li C, Zhao WF, Zhang Q, et al. Post-crosslinking towards stimuli-responsive sodium alginate beads for the removal of dye and heavy metals. *Carbohydr Polym*. 2015;133:587–95. Available from: <DOI>.
31. Kulig D, Zimoch-Korzycka A, Jarmoluk A, Marycz K. Study on alginate-chitosan complex formed with different polymers ratio. *Polymers*. 2016; 8(5): 167. Available from: <DOI>.
32. Li L, Zhao J, Sun Y, Yu F, Ma J. Ionically cross-linked sodium alginate/κ-carrageenan double-network gel beads with low-swelling, enhanced mechanical properties, and excellent adsorption performance. *Chem Eng J*. 2019;372(February):1091–103. Available from: <DOI>.
33. Abd El-Latif MM, El-Kady MF, Ibrahim AM, Ossman ME. Alginate/polyvinyl alcohol - kaolin composite for removal of methylene blue from aqueous solution in a batch stirred tank reactor. *J Am Sci*. 2010;6(December 2014):280–92. Available

from: <URL>.

34. Lafi R, ben Fradj A, Hafiane A, Hameed BH. Coffee waste as potential adsorbent for the removal of basic dyes from aqueous solution. *Korean J Chem Eng.* 2014 Nov 28;31(12):2198–206. Available from: <DOI>.

35. Liu T, Li Y, Du Q, Sun J, Jiao Y, Yang G, et al. Adsorption of methylene blue from aqueous solution by graphene. *Colloids Surfaces B Biointerfaces.* 2012;90(1):197–203. Available from: <DOI>.

36. Yürekli Y. Determination of adsorption capacities of NaX Nano-particles against heavy metals and dyestuff. *J Fac Eng Archit Gazi Univ.* 2019;34(4):2113–24. Available from: <DOI>.

37. Polat H, Zeybek N, Polat M. Tissue engineering applications of marine-based materials. *Marine Biomaterials.* 2022;205–54. Available from: <DOI>.

38. Günay A, Dikmen S, Ersoy B, Evcin A. Adsorption of Basic Blue-16 Dye onto Clay. *Environ Eng Manag J.* 2014;13(2):395–405. Available from: <URL>.

39. Xu J, Tian Y, Li Z, Tan BH, Tang KY, Tam KC. β -Cyclodextrin functionalized magnetic nanoparticles for the removal of pharmaceutical residues in drinking water. *J Ind Eng Chem.* 2022;109:461–74. Available from: <DOI>.

40. Civan Çavuşoğlu F, Akan S, Arı EA, Çetinkaya E, Çolak E, Daştan GN, et al. Preparation of magnetic activated carbon-chitosan nanocomposite for crystal violet adsorption. *Korean J Chem Eng.* 2019;36(11):1915–21. Available from: <DOI>.

41. Dada A.O, Olalekan A.P, Olatunya, A.M, Dada O. Langmuir, Freundlich, Temkin and Dubinin-Radushkevich Isotherms Studies of Equilibrium Sorption of Zn^{2+} Unto Phosphoric Acid Modified Rice Husk. *IOSR J Appl Chem.* 2012;3(1):38–45. Available from: <DOI>.

42. Pormazar SM, Dalvand A. Adsorption of Reactive Black 5 azo dye from aqueous solution by using amine-functioned Fe_3O_4 nanoparticles with L-arginine: Process optimisation using RSM. *Int J Environ Anal Chem.* 2022 Jun 21;102(8):1764–83. Available from: <DOI>.

43. Alamin NU, Khan AS, Nasrullah A, Iqbal J, Ullah Z, Din IU, et al. Activated carbon-alginate beads impregnated with surfactant as sustainable adsorbent for efficient removal of methylene blue. *Int J Biol Macromol.* 2021;176:233–43. Available from: <DOI>.

44. Ravi, Pandey LM. Enhanced adsorption capacity of designed bentonite and alginate beads for the effective removal of methylene blue. *Appl Clay Sci.* 2019;169(October 2018):102–11. Available from: <DOI>.

45. Rocher V, Siaugue JM, Cabuil V, Bee A. Removal of organic dyes by magnetic alginate beads. *Water Res.* 2008;42(4–5):1290–8. Available from: <DOI>.

46. Li C, Lu J, Li S, Tong Y, Ye B. Synthesis of Magnetic Microspheres with Sodium Alginate and Activated Carbon for Removal of Methylene Blue. *Materials (Basel).* 2017 Jan 20;10(1):84. Available from: <DOI>.

47. Eltaweil AS, Mamdouh IM, Abd El-Monaem EM, El-Subruiti GM. Highly efficient removal for methylene blue and Cu^{2+} onto UiO-66 metal-organic framework/carboxylated graphene oxide-incorporated sodium alginate beads. *ACS Omega.* 2021 Sep 14;6(36):23528–41. Available from: <DOI>.

